

# THE 4TH INTERNATIONAL CONFERENCE ON ALUMINUM ALLOYS

## K-R CURVES OF 2090 HIGH STRENGTH TEMPER THIN SHEETS

R. Doglione<sup>1</sup>, E. Ilia<sup>2</sup>, D. Firrao<sup>1</sup>

1. Dipartimento di Scienza dei Materiali e Ingegneria Chimica,  
Politecnico di Torino, Torino, Italy

2. Fergat, Rivoli, Italy

### Introduction

Among Al-Li alloys, AA 2090 was developed to achieve comparable strength, higher elastic modulus and lower density than the most used high strength aircraft structural alloy, namely the 7075-T6. In this respect, the best results are usually obtained by the T8 temper, which foresees cold work forming interposed between quench and ageing. Mechanical characteristics of rolled, forged and extruded 2090 alloy in the T8 temper are known. Moreover, 2090-T8 alloy fracture resistance properties have been widely examined under the LEFM approach, with a wide range of  $K_{IC}$  values determined for several product forms, namely plates, forgings, extrusions.

In spite of the fact that for these products an excellent nominal plane strain fracture toughness at ambient and criogenic temperature has been reported, the fracture behavior of thin sheets (2090-T83) is still under investigation. It has been demonstrated that unrecrystallized peak aged 2090 plate alloy (T81) is characterized by a delamination toughening coupled with a transgranular failure mechanism, which ensures high toughness and always global stable crack growth [1, 2, 3]. On the other hand, it has been pointed out that recrystallized 2090-T83 thin sheet (1.6 mm thick) displays an intergranular failure mechanism and quasistable fracture only at the onset of crack propagation [4].

Till now, K-R curves determinations have been scarce, with very few reported data [2, 4, 5, 6, 7]. Moreover, the correlations between fracture mechanisms and R-curves are limited [4, 5, 6], as well as the explanation of the curves on the basis of microstructural parameters. Owing to the fact that the knowledge of the plane strain fracture toughness is not apt to characterize thin aeronautical components, the general problem of the raising toughness (K-R-curves) of 2090 high strength tempers thin sheet is then posed. In order to clarify the problem, and to explore possible alternatives to the T8 temper [8], two different thermomechanical heat treatment were chosen: the usually adopted T83 temper and the T62 one. In both cases the alloy is peak aged, but in the latter one artificial ageing follows soon after quenching, without intermediate stretching.

## Experimental

AA 2090-T83 was received by Alcoa in the form of 1.6 mm thick sheet. Part of the lot was than subjected to a complete T62 heat treatment. Details on the thermomechanical treatments are given in Table 1.

Table 1. Details of the T83 and T62 tempers for 2090 alloy.

	solubilization temperature [°C]	deformation [%]	ageing temperature [°C]	ageing time [h]
T83	548	6	160	24
T62	548	-	190	24

Tension tests were performed in both L and LT directions under strain control at strain rates of  $10^{-4}$  and  $2 \times 10^{-5} \text{ s}^{-1}$ . The average results are reported in Table 2.

For fracture toughness tests, taking into proper consideration the sheet thickness, it was decided to fabricate 100 mm wide M(T) specimens; both tempers were tested in the LT and TL directions. The single specimen method coupled with the secant reciprocal slope technique was employed, according to the ASTM E561-86 Standard. Tests were performed under crack opening displacement control. This provides a decreasing crack growth driving force, which allows to follow a ductile fracture process entirely, thus limiting the possibility of global instability arising.

The microstructure was analyzed on metallographic samples by optical microscopy. Finally, the failure mechanism was studied on the fracture surfaces by microfractographic observations.

## Results

Metallographic analyses indicate for both tempers a fine recrystallized grain structure. The T62 temper is characterized by an equiaxed grain (aspect ratio close to unit), with a 5-10  $\mu\text{m}$  average grain diameter, whereas T83 temper has slightly elongated grains (aspect ratio between 1 and 1.5) again with 5-10  $\mu\text{m}$  average diameter, measured in the direction perpendicular to rolling. The rolling direction is also noticeable since it yields alignment along the grain boundaries of Al, Cu, Li, Fe, Si intermetallic compounds.

Stress-strain curves exhibit modest amplitude serrated plastic flow. This effect is more evident in the slower strain rate tests, and no noticeable differences are detectable either in different directions or tempers. On the other hand, mechanical tensile characteristics do not clearly show strain rate sensitive effects in the tested strain rate range. Accordingly, only averaged values were reported in Table 2. Tensile test results show once more the attractive stiffness properties of 2090 alloy: the normal elastic modulus at the 78000 MPa level throughout.

Table 2. Tensile characteristics of T83 and T62 tempers. Stress and Young's modulus values are given in MPa.

	E	$\sigma_{YS}$	$\sigma_{TS}$	e[%]
<b>T83</b>				
L	77,700	530	559	7
LT	78,500	506	537	10
<b>T62</b>				
L	78,300	467	522	4
LT	78,000	416	477	7

T62 temper obviously yields lower tensile resistance properties than the T83 one. This is an already known effect [9, 10], which is related to an enhanced  $T_1$  particles nucleation on the dislocations introduced by stretching in the T83 temper. Owing to the ensuing dramatic increase in the aging kinetics, it is possible in the T83 temper to lower the ageing temperature, thus reaching higher both  $T_1$  particles volume fraction and density number. Another interesting result following from stretching before ageing, is the increase in the tensile elongation, as reported in Table 2.

Load-crack opening displacement (P-COD) data obtained during fracture mechanics tests indicate that both tempers are characterized by several and, at times, large pop-in steps. The material shows a globally stable behaviour only at the beginning of the crack growth, and it has been impossible to control the fracture process along the hypothetical decreasing part of the load-crack opening displacement (P-COD) diagram. Moreover, a noticeable variability was found in the location of the failure point on the P-COD diagram: sometimes it happened quite before achieving horizontal tangency, sometimes near it and occasionally beyond the maximum load usually following a large pop-in. The degree of thickness constraint evolves, in both tempers, from full plane strain in early stages of loading and crack propagation up to full plane stress, with macroscopic slant fracture morphology. Plane stress zones, either partially occupying the specimen thickness or encompassing the full thickness, are prone to sudden failure which gives rise to pop-in occurrence and stepped K-R curves, see Figures 1 and 2.

#### Discussion

The K-R curves reported in Figures 1 and 2 show some peculiar characteristics, namely the grouped distribution of points spaced by pop-ins more visible in the upper part of the curves. Here, after pop-in and crack arrest, new low elevation high K level blunting occurs. In the case of the TL direction, for both tempers, a more pronounced tendency toward instability is verified and the toughness plateau is less defined, even if occasionally crack arrest occurs after a very large pop-in (Figure 2). However, the test ends always with unstable fracture: the toughness plateau is reached but not maintained so that after a few pop-ins the crack propagates catastrophically. It emerges that in both tempers the final collapse points are either located in the rising portion of the K-R curve or after a toughness plateau has been substantially described. Ascribing the former occurrence as a statistically unreliable behaviour of the material,

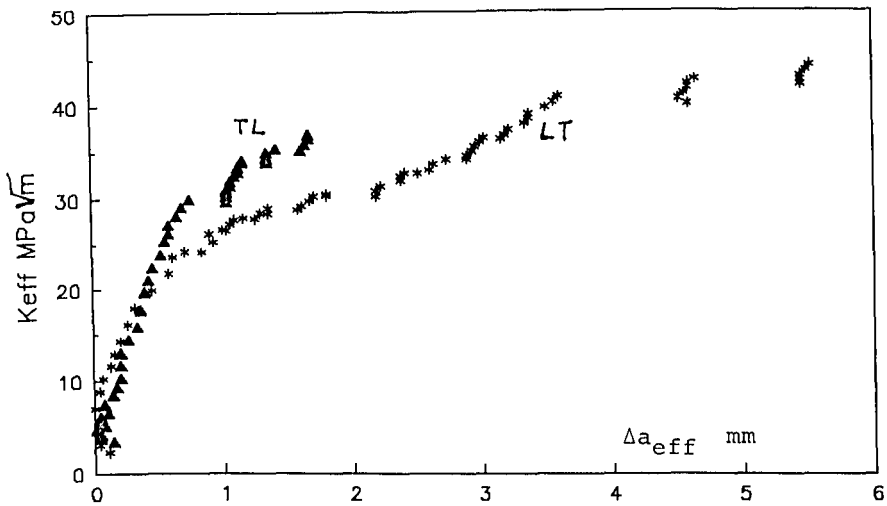


Figure 1.  $K_{eff}-\Delta a_{eff}$  curves for 2090-T83 alloy tested in the TL and LT directions.

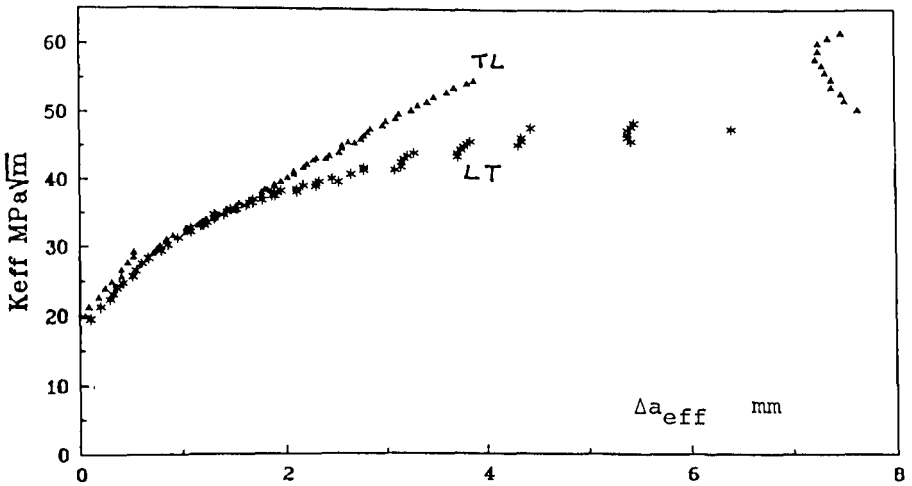


Figure 2.  $K_{eff}-\Delta a_{eff}$  curves for 2090-T62 alloy tested in the TL and LT directions.

the toughness plateaus are a reasonable estimate of the maximum level of toughness that can be eventually achieved by the two different heat treated materials. Thus, for the sake of comparison, these plateau levels, here termed  $K_{\infty}$ , have been taken as a significant estimate of the fracture resistance. Obviously,  $K_{\infty}$  are not to be incorporated in any design code, given the already described scatter in the material behaviour. The average values of  $K_{\infty}$  are then reported in Table 3.

Table 3: average toughness plateau levels  $K_{\infty}$  (MPa $\sqrt{m}$ ).

	T83-LT	T83-TL	T62-LT	T62-TL
$K_{\infty}$	43	36	47	53

In order to explain the differences in the  $K_{\infty}$  values upon changing heat treatment and loading direction, an examination of the fracture mechanism and its correlation with the microstructure is necessary. For both tempers and directions, in the first small part of crack growth (about 50-100  $\mu$ m) fracture occurs in central plane strain zones, mainly by the classical microvoids nucleation and coalescence around coarse equilibrium intermetallic compounds, mainly located at the grain boundaries. At this stage, the propagation is quasistatic along the entire defect front. Quasistatic fracture continues in the central plane strain zones which narrow up to form a flat fracture zone very similar to a tongue, Figure 3. Now also localized crystallographic slip becomes important and, owing to the presence of  $\delta'$  particles which concentrate slip into narrow bands, the fracture surface is characterized by microvoids joined by areas of transgranular shear. Subsequently, the plane stress lateral zones suddenly

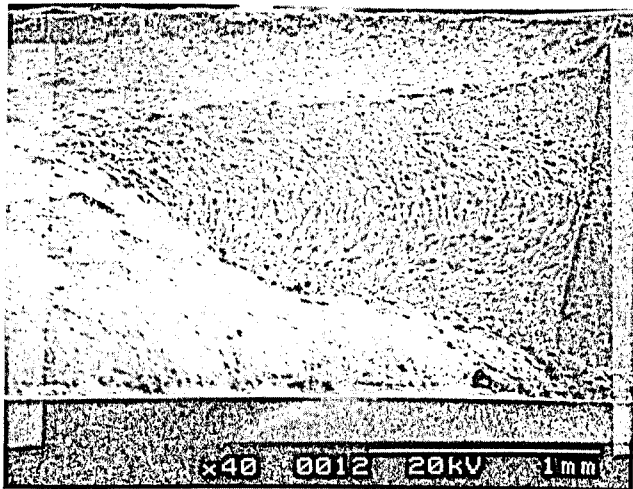


Figure 3: typical macroscopical fracture morphology, with central plane strain flat tongue and lateral plane stress slant surfaces.

collapse causing the appearance of limited pop-ins; here the fracture is macroscopically dominated by transgranular shear along coarse and planar slip bands.

Referring to Figure 3, there is a correspondance between the achievement of the toughness plateaus on the K-R curves and the last part of the flat tongue and adjacent lateral slant fractures. Comparing fracture morphologies of T83 and T62 tempers, no substantial differences were noticed at the tongues, whereas in the lateral zones pronounced intergranular decohesion characterizes the T83 temper; instead, in the T62 heat treated alloy the usual adiabatic shear predominates in the slant portion of fracture, Figure 4 and 5. The outlined differencies can explain the T62 higher toughness plateau.

Further observation on the fracture mechanism allow the explanation of the final uncontrollable failure. The morphology of the intergranular fracture and the transgranular shear is changing as the crack velocity progressively accelerates during the catastrophic failure. At lower crack propagation rates, immediately after the onset of the final event, the failed fracture surfaces are covered with a fine dimpled structure, which corresponds to ductile failure around intermetallic particles. At high strain rates verified during fast crack propagation, plastic deformation and microvoids formation are reduced and substituted by almost smooth fracture surfaces. Furthermore, upon increasing the crack growth velocity, shear strains localization bands narrow to the point that they are reduced to a thin blade of deformed material so that shear fracture surfaces are very smooth in the T62 temper thus causing a low global ductility. On the contrary, a predominantly brittle intergranular fracture emerges for T83, thus pointing out a grain boundary embrittling phenomenon.



Figure 4: ductile transgranular shear fracture in plane stress zones (T62 temper TL direction)

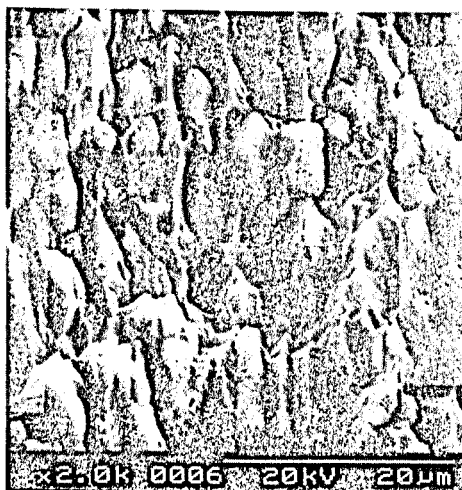


Figure 5: brittle intergranular fracture in plane stress zones (T83 temper T1 direction)

As already suggested in [6], the local instability phenomena can be explained in terms of local tearing instability. In general, tearing instability means that the applied tearing modulus exceeds the material tearing modulus. In crack opening control, and if the local collapse mechanism is unique, this may not occur. In the present material, the progressive disappearance of microvoids as crack accelerates, imply a variation in the rate of absorbed energy, giving rise to a local material tearing modulus variation and then to local instability. Moreover, from tension tests and P-COD diagrams clear evidences of strain rate sensitivity of the material appear, confirmed by the variation of the fracture morphology as crack accelerates.

The complex combination of all the above outlined factors dictates the fracture behaviour of the alloy. Here the tearing modulus criterion, applied to a fracture mechanism change, predict only the onset of instability, whereas in crack opening displacement control, it cannot predict a global instability. In fact, in the present case, the applied tearing modulus is lowered by the constant COD rate control and the crack maybe stopped. Global instability is then to be predicted by a global elastic energy balance, i.e. the K-R curve. For the 2090-T83 or T62 alloy, the fracture mechanism changes and the strain rate effects accompanying crack growth acceleration, pull down the energy rate absorption, finally resulting in a global instability. Here the role of the last local plastic instability is to trigger the onset of global elastic instability, what once more points out a certain degree of strain rate sensitivity of the material.

A comparison between T83 and T62 tempers and an explanation of the different toughness can be attempted. First of all, the superior toughness coupled with T62 temper is surprising. In the 2000 series Aluminium alloys, and particularly in Al-Li alloys, it is commonly believed that T8 temper guarantees not only superior strength but also superior toughness compared to T6 one [1]. This is explained by the fact that stretching before ageing (T8) leads to an enhanced  $T_1$  particles nucleation on the dislocations: it is believed that this prevents grain boundaries precipitation and hinders slip localization. Here, the higher grain boundary brittleness of the T83 temper, as showed by fractographic analyses, contrasts with this conclusion. Possible explanation of this fact is that during the T62 second solubilization, preexisting grain boundaries precipitates not dissolved by the first (T83) heat treatment, go further into solid solution, counterbalancing the subsequent tendency to grain boundary precipitation during ageing. The second important fact is that toughness anisotropy is reversed by T62 heat treatment, being TL direction tougher than LT one, in contrast with T83 temper. Again the possible explanation arise from the second solubilization: in this stage recrystallization strengthens the recrystallization texture (Cube and Goss) at the expense of the preexisting rolling texture (Brass, S and Copper) [11], marginally reduced by the first heat treatment.

### Conclusions

K-R curves have been determined for both 2090-T83 and 2090-T62 thin sheet alloy, performing tests in crack opening displacement control. Their aspect was explained in terms of fracture mechanism. It was found that the material displays a collapse mechanism change from high ductility to low ductility in

the T62 heat treatment and even to an intergranular brittle morphology in the T83 temper. Global final instability is achieved in both cases, which is accompanied by a certain degree of fracture unreliability. Related to this fact, a certain degree of strain rate sensitivity of the material has been pointed out. A comparison between T83 and T62 tempers shows higher tensile characteristics for the former, which displays, instead, a lower toughness in respect to the latter, due to its tendency to brittle intergranular slant fractures.

#### References

1. K.T. Venkateswara Rao, R.O. Ritchie, Material Science and Technology 5 (1989), 882.
2. K.T. Venkateswara Rao, R.O. Ritchie, 5th International Aluminium-Lithium Conference, ed. T. H. Sanders Jnr and E. A. Starke Jnr (Materials and Component Engineering Publications Ltd., Birmingham, UK, 1989), 1501.
3. K.T. Venkateswara Rao, R.O. Ritchie, Acta Metall. Mater. 38, (1990), 2309.
4. R.J.H. Wanhill, L. Schra and W.G.J. Hart, 6th International Aluminium-Lithium Conference, ed M. Peters and P. J. Winklers (DGM Informationsgesellschaft Verlag, Oberursel, Germany, 1992) 253.
5. R. Doglione, E. Ilia, D. Firrao, Proc. VII Convegno Nazionale Gruppo Italiano Frattura, ed.S. Reale (Firenze, Italy, 1991), 57.
6. R. Doglione et al., Int. Conf. Materials Development in Rail, Tire, Wing, Hull Transportation, (Genova, Italy, 1992) 1.191.
7. G. Cavallini et al., New Light Alloys, (AGARD n. 444, Neuilly sur Seine, France, 1989), 11-1.
8. P.E. Bretz, 4th International Aluminium Lithium Conference, ed. G. Champier et al., J. de Physique, Tome 48, Colloque C3, suppl. au n. 9, (1987), C3-25.
9. L. Blackburn et al., Aluminum-Lithium Alloys, Design, Development and Applications Update, ed. R. J. Kar et al., (ASM, Los Angeles, California, 1987), 187.
10. W. A. Cassada, G. J. Shiflet and E. A. Starke Jr., Met. Trans. 22A, (1991), 299.
11. A. K. Vasudevan, M. A. Przystupa and W. G. Fricke, Jr., Scripta Metall. et Mater. 24, (1990), 1429.